AIAA JOURNAL
Vol. 44, No. 7, July 2006

Computational Analysis of Gravitational Effects in Low-Density Gas Jets

Rajani P. Satti
University of Oklahoma, Norman, Oklahoma 73019
and
Ajay K. Agrawal*
University of Alabama, Tuscaloosa, Alabama 35487

DOI: 10.2514/1.12825

This study deals with the computational analysis of the near-field flow structure in an isothermal helium jet injected into quiescent ambient air environment. Laminar, axisymmetric, and unsteady flow conditions were considered for the analysis. The transport equations of helium mass fraction coupled with the conservation equations of mixture mass and momentum were solved using a staggered grid finite-volume method. Jet Richardson numbers encompassing both buoyant and inertial jet flow regimes were considered. Buoyancy effects were isolated by initiating computations in Earth gravity and subsequently, reducing the gravity to simulate microgravity conditions in the 2.2 s drop tower. Computed results concur with experimental observations, i.e., a self-excited buoyant jet with periodic flow oscillations in Earth gravity becomes steady in microgravity. In an inertial jet, the flow oscillations occur at the same frequency regardless of the buoyancy, although the oscillation amplitude decreases in microgravity.

I. Introduction

LOW-DENSITY gas jets are characterized by the injection of a lighter fluid into a dense ambient environment. The resulting flow structure is susceptible to buoyancy arising because of the difference in densities of jet and surrounding fluids. In general, jets are considered buoyant for jet Richardson number, $Ri = gd(\rho_\infty - \rho_j)/\rho_j U_j^2 > 1.0$ and inertial for $Ri \ll 1.0$, where g is the gravitational acceleration, d is the injector tube inside diameter, ρ_∞ and ρ_j are, respectively, the ambient and jet fluid densities, and U_j is the average jet exit velocity. The present study examines low-density gas jets in both buoyant and inertial flow regimes, with the goal of delineating gravitational effects on the flow structure in the near-field.

Several studies [1–6] have focused on the far-field behavior of low-density jets, which is influenced by the processes in the near-field. Low-density gas jets are known to exhibit self-excited periodic oscillations in the near-field in both buoyant and inertial flow regimes. In the buoyant flow regime, Subbarao and Cantwell [7] conducted experiments with helium jets injected into a coflow of air for Ri varying from 0.5 to 6.0. The frequency f of the periodic oscillations expressed by the Strouhal number, $Sr = fd/U_j$ correlated with the jet Richardson number for $Ri > 1.0$ indicating buoyancy dependent instability. Hamins et al. [8] observed periodic oscillations in helium jets injected into air, and reported that a minimum jet exit velocity is required to initiate the oscillations. Similar experiments were conducted by Cetegen and Kasper [9] and Cetegen [10,11] in axisymmetric and planar plumes, whereby buoyancy induced toroidal vortical structures contaminating the primary jet flow were observed. Diagnostics involved velocity measurements using laser Doppler velocimetry and particle image velocimetry. Pasumarthi and Agrawal [12] conducted experiments to characterize the jet flow by concentration measurements across the whole field of a helium jet injected into quiescent air. Experiments by Yep et al. [13] demonstrated that the self-excited flow oscillations in Earth gravity were absent in the microgravity environment of the 2.2 s drop tower at the NASA Glenn Research Center.

Self-excited oscillations have also been reported in low-density inertial jets for $Ri \ll 1.0$ [14–17]. In these studies, the jet Richardson number was small, and hence, buoyancy was considered negligible. Although this assumption is justified within the jet core, buoyancy could be important in the jet shear layer where the density and velocity gradients are large. Experiments by Yildirim and Agrawal [18] show significant buoyancy effects on flow oscillations and transition to turbulence in high-momentum helium jets. Recently, Pasumarthi [19] conducted experiments in the 2.2 s drop tower using helium jets injected into quiescent air for $Ri < 1.0$. Concentration measurements revealed global self-excited oscillations in the near-field in Earth gravity. In microgravity, the oscillation amplitude decreased for $Ri < 0.01$ and no oscillations were observed for $Ri > 0.1$. These experiments provide direct physical evidence of significant buoyancy effects in low-density gas jets over a range of jet Richardson numbers. Results by Pasumarthi and Agrawal [20] show differences in the flow structure and transition behavior with the change of gravity in the drop tower.

Previous experiments have characterized buoyancy effects using either concentration or velocity measurements. However, simultaneous visualization of velocity and concentration fields is desired to fully understand the dynamics of the oscillating flow structure. Experimental difficulties in obtaining simultaneous vector-scalar measurements, especially in the low-gravity environment, have prompted studies of gas jets using computational fluid dynamic (CFD) analysis. Mell et al. [21] performed numerical simulations of helium jets injected into air and found that the computed flow oscillation frequency matched with experiments of Hamins et al. [8]. Recently, Soteriou et al. [22] investigated the near-field dynamics of planar buoyant plumes incorporating a Lagrangian transport element method. Computations qualitatively captured the plume instantaneous behavior observed in experiments. The mechanism of vorticity generation and relative roles of buoyancy and viscous forces in explaining the plume instability were discussed. Structural details of the buoyant low-density gas jets were analyzed computationally by Satti and Agrawal [23]. On a related note, several numerical studies have been conducted to understand the dynamics of flickering jet diffusion flames [24,25].

Received 19 August 2004; revision received 15 March 2006; accepted for publication 13 February 2006.

*Robert F. Barfield Endowed Chair Professor, Department of Mechanical Engineering; aagrawal@eng.ua.edu. Senior Member AIAA (corresponding author).

Table 1 Transport coefficients and source terms in Eq. (2)

Variable	ϕ	Γ^ϕ	S^ϕ
Axial velocity	w	μ	$-r\frac{\partial p}{\partial z}+r(\rho_\infty-\rho)g+\frac{\partial}{\partial z}(r\mu\frac{\partial w}{\partial z})+\frac{\partial}{\partial r}(r\mu\frac{\partial v}{\partial z})-\frac{2}{3}[\frac{\partial}{\partial z}(r\mu\frac{\partial v}{\partial r})+\frac{\partial}{\partial z}(r\mu\frac{\partial w}{\partial r})]$
Radial velocity	v	μ	$-r\frac{\partial p}{\partial r}-\frac{2}{3}\mu\frac{v}{r}+\frac{\partial}{\partial z}(r\mu\frac{\partial w}{\partial r})+\frac{\partial}{\partial r}(r\mu\frac{\partial v}{\partial r})-\frac{2}{3}[\frac{\partial}{\partial r}(r\mu\frac{\partial v}{\partial r})+\frac{\partial}{\partial r}(r\mu\frac{\partial w}{\partial z})]$
Helium mass fraction	f	ρD_b	0

The preceding literature review reveals that the previous computational studies have not delineated the effects of buoyancy in low-density gas jets. In the present study, both buoyant and inertial jets are examined in Earth gravity, microgravity, and during the change from Earth to microgravity. The CFD analysis is used to concurrently visualize velocity and concentration fields, a difficult experimental task, especially in the constrained environment of the microgravity facilities. By analyzing instantaneous and time-averaged velocity and helium concentration fields over a range of jet Richardson numbers, this study aims to explore the physical implications of the self-excited instability in low-density gas jets.

II. Numerical Formulation

A. Governing Equations

Consistent with experimental studies, the numerical formulation is based on unsteady, laminar, and axisymmetric flow behavior. The unsteady analysis is necessary to capture the self-excited oscillations observed in low-density gas jets. The flow is laminar in the near-field because the maximum jet Reynolds number is 800. Experiments by Cetegen and Kasper [9] show flow asymmetry and 3-D effects in the near-field, especially at high jet Richardson numbers. However, in the jet Richardson number range of the present study, excellent flow symmetry has been documented experimentally in both buoyant [7–12] and inertial jets [16,18,19]. The following approximations were made to simplify the analysis: 1) the flow is incompressible, 2) temperature and pressure variations are negligible, and 3) the flow is a binary fluid system with air treated as a single species. The justification for these simplifications is discussed by Kyle [26]. Accordingly, the governing equations are expressed as follows:

$$\frac{\partial \rho}{\partial t}+\frac{1}{r}\frac{\partial}{\partial r}(\rho v r)+\frac{\partial}{\partial z}(\rho w)=0 \tag{1}$$

$$\frac{\partial(\rho r\phi)}{\partial t}+\frac{\partial}{\partial r}(\rho v r\phi)+\frac{\partial}{\partial z}(\rho r w\phi)=\frac{\partial}{\partial r}\left(\Gamma^\phi r\frac{\partial \phi}{\partial r}\right)+\frac{\partial}{\partial z}\left(\Gamma^\phi r\frac{\partial \phi}{\partial z}\right)+S^\phi \tag{2}$$

Equation (1) represents the continuity equation and Eq. (2) is the generalized transport equation, which represents the momentum, or species conservation equation depending on the variable ϕ. Γ^ϕ and S^ϕ are, respectively, the transport coefficient and source term of the variable ϕ, as listed in Table 1.

Density was computed from the equation of state for incompressible ideal gas. The dynamic viscosity was calculated using Wilke's mixture averaged formula [27]. Following Gaenkoplis [28], the binary diffusion coefficient of helium into air, D_b, was specified as a constant. Higher level models including the multicomponent diffusion model were also tested. However, they produced the same results. In the 2.2 s drop tower, the gravity changes linearly from Earth gravity to microgravity within 0.1 s after the drop. The gravitational acceleration in microgravity is $100\mu g$, where g is Earth's gravitational acceleration. The computations replicated these features of the drop tower to simulate the evolving flow structure of the jet during the drop.

B. Boundary Conditions

The computational domain extended 15.0 d in the axial direction and 6.0 d in the radial direction. These dimensions were established after trials using domains of different sizes such that the near-field flow behavior was independent of the domain size. The upstream boundary was placed at a distance of 1.0 d from the jet exit plane to account for the upstream diffusion observed in experiments [12]. The flow symmetry was imposed along the jet centerline. At the tube inlet, the axial velocity profile was fully developed and the helium mole fraction was unity. No slip and zero mass diffusion conditions were imposed on the inside and outside walls of the tube. Exit boundary was specified as pressure outlet, whereby the exit flow properties were extrapolated from the interior. Pressure inlet and pressure outlet conditions were specified, respectively, at the upstream and far-field radial boundaries. All of the flow properties were set to zero at the start of the computations to simulate the evolving flow structure from a stationary state. The operating pressure and temperature were specified, respectively, as 1.0 atm and 300 K.

C. Computational Procedure

An orthogonal nonuniform grid system was used to split the computational domain into five subregions. The grid points in the radial direction were concentrated in the shear layer region. The grid size was increased gradually in the axial direction. The governing equations were solved sequentially using a segregated approach with pressure-velocity coupling provided by the SIMPLEC algorithm [29]. Grid sensitivity analysis was performed to obtain grid-independent solution requiring 30,000–80,000 nodes depending upon the jet Richardson number. Convergence tests using different time steps were performed to accurately resolve the flow oscillation frequency. Computations for the inertial jet required a higher number of grid nodes and a smaller time step compared with those for the buoyant jet. No external perturbations were imposed to initiate the flow oscillations.

D. Validation

Several test cases were computed to validate the numerical model used in this study. First, the computations were compared with scalar measurements of a steady helium jet in air [30]. The results presented in [23] showed that the numerical model accurately simulated the diffusion process in low-density gas jets. Next, computations were performed over a range of jet Richardson numbers to compare the flow oscillation frequency with the experimental correlation given by Hamins et al. [8]. Results in Fig. 2b of [23] show an excellent agreement between measurements and computations, proving the reliability of the model in predicting the complex features of the oscillating flow in low-density jets over a range of jet Richardson numbers.

III. Results and Discussion

Time-dependent simulations of the isothermal helium jet injected into ambient air were performed with the objective of quantifying buoyancy effects in the near-field. Although the computations were performed for several cases, detailed results are presented only for one buoyant jet and one inertial jet at test conditions listed in Table 2. First, details pertaining to the flow behavior of a buoyant jet in Earth

Table 2 Summary of test conditions

Case	Re	Ri	d, mm	U_j, m/s	Grid size	Time step, ms
Case 1 (buoyant)	300	1.52	31.8	1.15	31,000	1.67
Case 2 (inertial)	800	0.018	14.5	6.75	81,000	0.30

gravity and during the change from Earth gravity to microgravity are presented. Similar information is provided for the inertial jet. Finally, the flow behavior of buoyant and inertial jets is compared in Earth gravity and microgravity.

A. Buoyant Jet

1. *Flow and Concentration Fields in Earth Gravity*

The jet flow evolved gradually from the stationary state and eventually exhibited periodic oscillations in the near-field at a unique frequency. Computations were continued for sufficiently long time such that the effects of initial conditions and numerical disturbances were flushed out. Specifically, the flow periodicity was ascertained by monitoring the flow structure for 50 consecutive cycles indicating no detectable change between cycles. Figure 1 shows a sequence of velocity vector plots superimposed with helium mole percentage contours during the oscillation cycle for the buoyant jet (Case 1). At $t = 0.0$ ms, buoyancy accelerates the jet core, which contracts to conserve the mass. This results in the entrainment of the ambient fluid to produce a toroidal vortex. Note that the vortex core represented by a dot in Fig. 1 is located at $z/d = 0.12$ for $t = 0.0$ ms.

In the next plot at $t = 13.3$ ms, the vortex is characterized by a larger recirculation region accompanied with greater contraction of the jet core, evident from the inward indentations in the concentration field near $z/d = 0.2$. Subsequently, between $t = 26.7$ and 55.1 ms, the vortex grows in size, convects downstream and contaminates a greater portion of the jet core. The vortex gains strength by transfer of the momentum from the jet core. This feature is evident in Fig. 1 wherein the velocity vectors downstream of the vortex core are larger than those upstream before interacting with the jet core. As the vortex propagates downstream, the jet expands near the tube exit to initiate another vortex at $t = 68.3$ ms to repeat the oscillation cycle. These results illustrate self-excited periodicity in the jet at a frequency of 14.6 Hz. Yep et al. [13] measured an oscillation frequency of 12.5 Hz at similar test conditions. However, the experiments by Yep et al. were performed in a drop rig with a short jet tube because of the severe space limitations. Thus, the flow at the jet exit was not fully developed, in contrast to the fully developed flow at the tube inlet specified for the computations. These differences in the inlet flow conditions must be considered when comparing the present results with measurements of Yep et al.

2. *Flow and Concentration Fields during the Change from Earth Gravity to Microgravity*

Computations were performed to visualize the jet flow during the change from Earth gravity to microgravity and to depict how the jet flow adjusts itself in microgravity. The simulations were compared with experiments [13] to verify the computational model in reduced gravity. Figure 2 shows a series of computational-experimental helium mole fraction contour plots during the change from Earth gravity to microgravity (as discussed, the gravity varies linearly during the first 100 ms). At the onset of the change denoted as $T = 0.0$ ms, the indentations in the helium concentration level higher than 50% signify a vortex located at $z/d = 0.7$. After 16.7 ms, the vortex convects downstream as the jet expands in the near exit region. At $T = 50.0$ ms, the jet has expanded at the exit to $r/d = 0.7$. The indentations in the concentration contours have weakened, signifying the diminishing nature of the vortex. Subsequently, the jet widens gradually throughout the near-field as steady conditions are reached in microgravity. The helium mole fraction contours in microgravity are straight lines reminiscent of a nonbuoyant jet. These

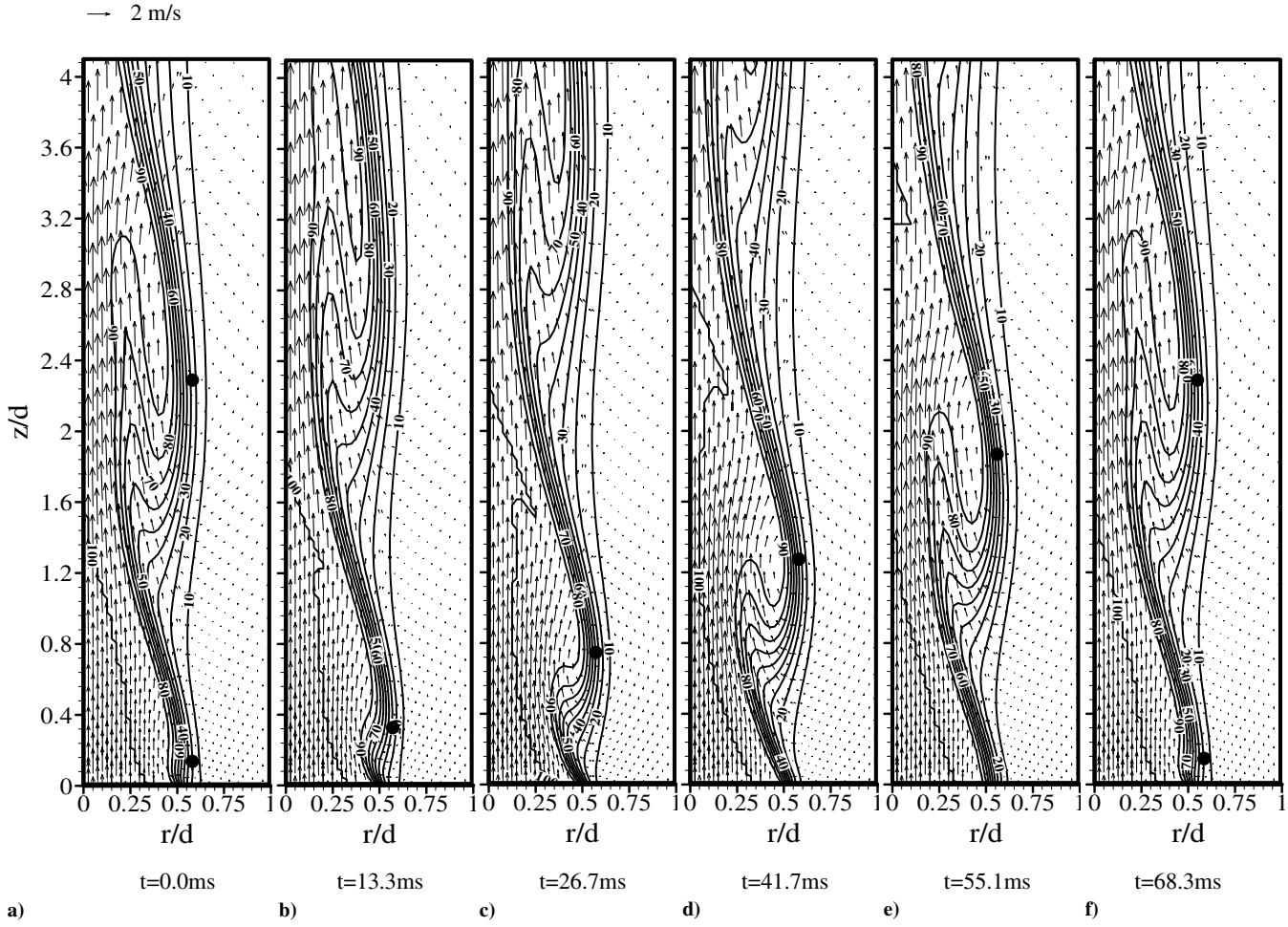

Fig. 1 Velocity vectors superimposed by contours of helium mole percentage during an oscillation cycle in Earth gravity for the buoyant jet: $Ri = 1.52$, $Re = 300$, $d = 31.8$ mm (Case 1).

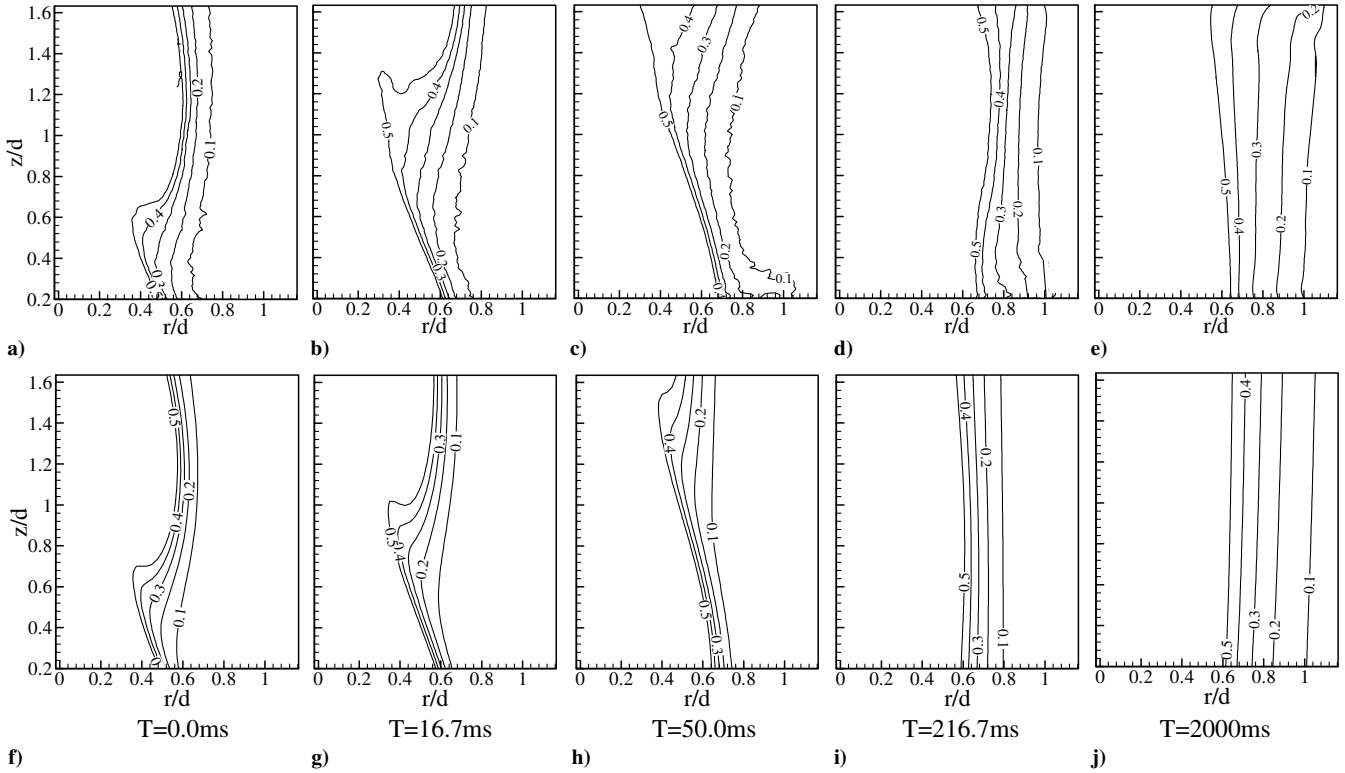

Fig. 2 Measured (2a–2e) and computed (2f–2j) helium mole fraction contours during the change from Earth gravity to microgravity for the buoyant jet: $Ri = 1.52$, $Re = 300$, $d = 31.8$ mm (Case 1).

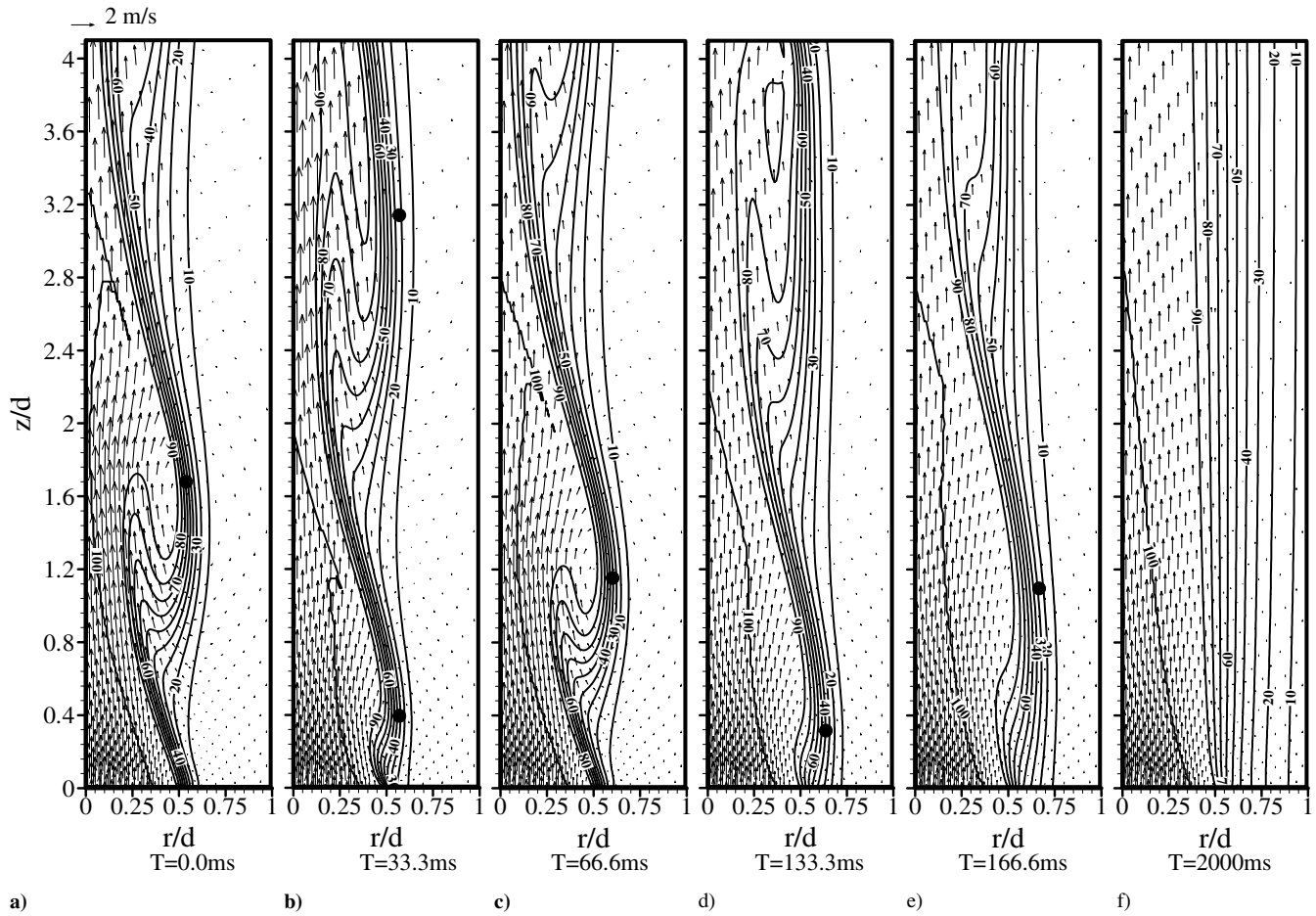

Fig. 3 Velocity vectors superimposed by contours of helium mole percentage during the change from Earth gravity to microgravity for the buoyant jet: $Ri = 1.52$, $Re = 300$, $d = 31.8$ mm (Case 1).

features replicate similar phenomena observed in experiments , i.e., the self-excited flow oscillations in Earth gravity subside in microgravity. Results in Fig. 2 show that the present model is effective in reproducing experimental features of the jet flow in the 2.2 s drop tower, although the radial diffusion was under-predicted.

Figure 3 shows velocity vectors superimposed by contours of helium mole percentage during the change from Earth gravity to microgravity to highlight the interaction between velocity and concentration fields. At $T = 0.0$ ms, a vortex with its center located at $z/d = 1.7$ characterizes the entrainment of ambient fluid into the jet core. Near the jet exit, the helium mole fraction is 10% at $r/d = 0.6$. At $T = 33.3$ ms, the jet at the exit has expanded to $r/d = 0.65$. The vortex has convected downstream with its center located at $z/d = 3.2$. At $T = 66.6$ ms, the vortex has moved downstream of the field-of-view while another vortex has formed at $z/d = 1.2$. In microgravity at $T = 133.3$ ms, the flow recirculation decreases and the jet expands to $r/d = 0.75$ near the exit. Figures 3b–3d show a gradual decrease in the indentations in the concentration contours as the buoyancy is reduced. Similar features are exhibited at $t = 166.6$ ms as the flow approaches steady state in microgravity. Finally, at $T = 2000$ ms the jet assumes steady columnar shape. Further details of the flow structure during the change from Earth gravity to microgravity are discussed next using the spatio-temporal plots.

3. *Temporal Evolution of Axial Velocity and Concentration Fields*

Figure 4 depicts the temporal evolution of the helium concentration field during the change from Earth gravity to microgravity. Computed and measured [13] time traces of helium mole fraction at $z/d = 1.0$ illustrate that the oscillating jet flow expands in the radial direction after the change in gravity. Results show that the oscillations sustain during a brief initial period of the change and steady conditions are reached within $T = 0.75$ s. Again, the experimental trends are predicted well by the computations. Figure 5 shows time trace plots of helium mole percentage and axial velocity at selected locations during the change in gravity. Near the jet exit at $z/d = 0.15$, pure helium was present at the jet center ($r/d = 0$) for all times. In contrast, the axial velocity at the jet center fluctuates between 2.3 and 2.6 m/s in Earth gravity. In microgravity, the axial velocity reaches a steady value of 2.2 m/s at $T = 0.2$ s. The reduction in the axial velocity with the change in gravity is small because the axial plane $z/d = 0.15$ is close to the jet exit. In the entrainment region at $r/d = 0.45$, the helium mole percentage in Earth gravity varies between 45 and 94%. During the change to microgravity, the helium concentration peaked almost to 100% within 0.08 s. Afterwards, minor variations occurred before a steady value of 95% was reached at $T = 0.3$ s. The corresponding axial

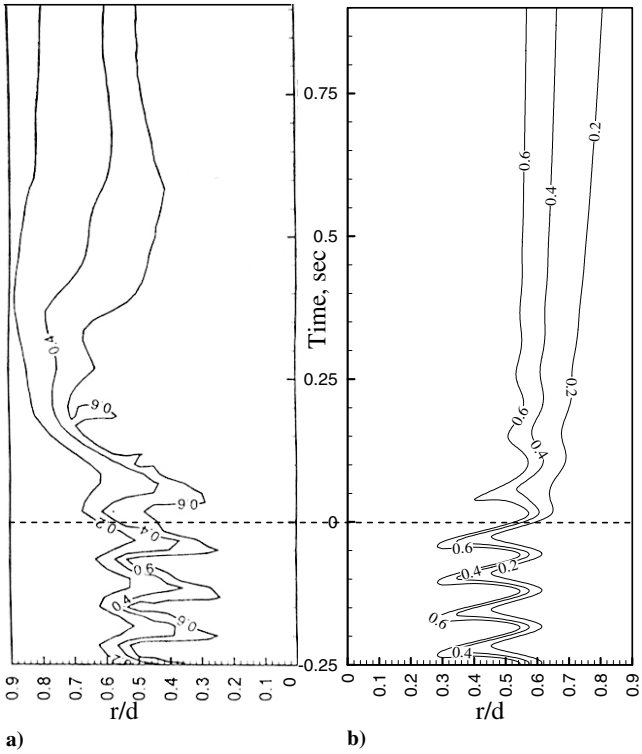

Fig. 4 a) Measured and b) Computed time traces of helium mole fraction during the change from Earth gravity to microgravity for the buoyant jet: $Ri = 1.52$, $Re = 300$, $d = 31.8$ mm (Case 1) at $z/d = 1.0$.

velocity in microgravity is 0.4 m/s. Near the jet boundary at $r/d = 0.6$, low amplitude oscillations in the concentration field occur in Earth gravity. In microgravity, the helium mole percentage reached a steady value of 50% within $T = 0.8$ s. In Earth gravity, the axial velocity profile at $r/d = 0.6$ shows negative velocities because of the flow recirculation.

At a downstream location, $z/d = 2.0$, pure helium is present at the jet center for all times. The axial velocity and its oscillation amplitude have increased at this location, signifying buoyant acceleration in Earth gravity. The flow oscillations diminish within 0.5 s of the change in gravity to result in steady axial velocity of 2.1 m/s. At $r/d = 0.45$, high amplitude concentration oscillations are observed in Earth gravity. At $r/d = 0.6$, helium reaches peak concentration level of 64% during the change in gravity and a steady value of 56% is attained at $T = 0.6$ s. Axial velocity profiles in Fig. 5d depict flow

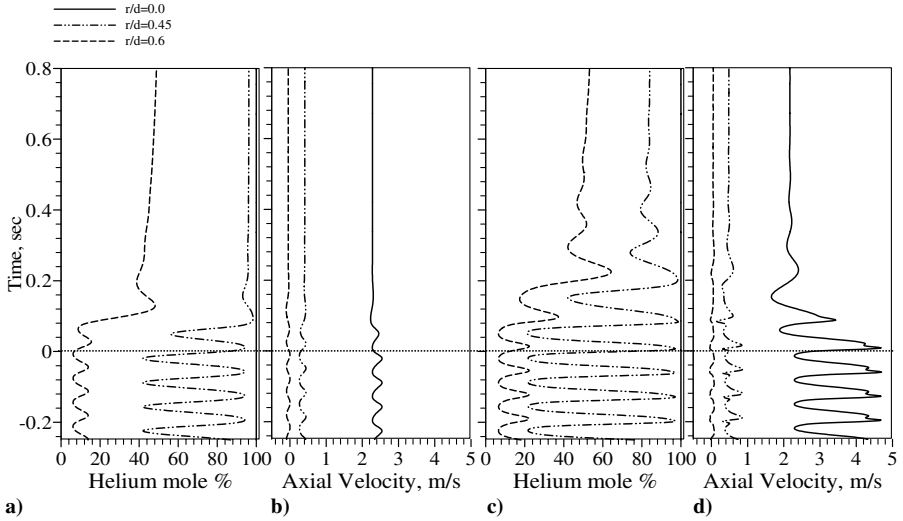

Fig. 5 Time traces of helium mole percentage and axial velocity during the change from Earth gravity to microgravity for the buoyant jet: $Ri = 1.52$, $Re = 300$, $d = 31.8$ mm (Case 1) at $z/d = 0.15$ (5a and 5b) and $z/d = 2.0$ (5c and 5d).

behavior similar to that observed upstream as shown in Fig. 5b. These features agree with time traces of the concentration field measured by Yep et al. [13].

B. Inertial Jet

1. Flow and Concentration Fields in Earth Gravity

Figure 6 shows a sequence of velocity vector plots superimposed with helium mole percentage contours to depict an oscillation cycle for the inertial jet. In this case, the computed results are presented between $r/d = 0.3$ and 0.65 to visualize the flow oscillation region in greater details. At $t = 0.0$ ms, buoyant acceleration contracts the jet core leading to entrainment and formation of the toroidal vortex. The flow structure including the nature and propagation of the toroidal vortex is similar to that of the buoyant jet in Fig. 1. The computed oscillation frequency was 150 Hz, compared with a frequency of 120 Hz measured in Earth gravity by Pasumarthi [19] in the drop rig. The deviation between computed and measured frequencies is attributed in part to the differences in the jet inlet conditions as discussed in preceding sections.

Although self-excited flow oscillations were observed in both buoyant and inertial jets, some aspects of the flow field are different. First, based on the concentration field, the inertial jet is wider compared with the buoyant jet. The contraction of the jet core and the mixing by entrainment are confined to a narrower region in the inertial jet compared with those in the buoyant jet. The oscillation frequency of the inertial jet is much higher (150 Hz) than that for the buoyant jet (14.5 Hz). Results illustrate self-excited periodicity in the flow field irrespective of the initial jet momentum, which agrees qualitatively and quantitatively with experiments [13,19].

2. Flow and Concentration Fields during the Change from Earth Gravity to Microgravity

Figure 7 shows velocity vector plots overlapped with contours of helium mole percentage during the change from Earth gravity to microgravity to highlight the interactions between velocity and concentration fields. At the onset of the change ($T = 0.0$ ms), a toroidal vortex is located at $z/d \cong 1.6$. This vortex convects downstream and a new one is observed at $z/d = 1.4$ at $T = 24.9$ ms. Subsequently, the jet flow attains a periodic structure in microgravity as depicted in Figs. 7c–7f. The curvature of the concentration contours is less severe and the vortex is narrower in microgravity. This result is consistent with experiments of Pasumarthi [19] showing a decrease in the flow oscillation amplitude in microgravity for $Ri < 0.01$. Computations in microgravity were performed for 20 oscillation cycles to ascertain the periodic nature of the flow oscillations. Results confirmed highly periodic oscillations at the same frequency in both Earth gravity and microgravity. Thus, even though the buoyancy affects the overall flow structure, the self-excited oscillations in the inertial gas jet occurred regardless of the gravity.

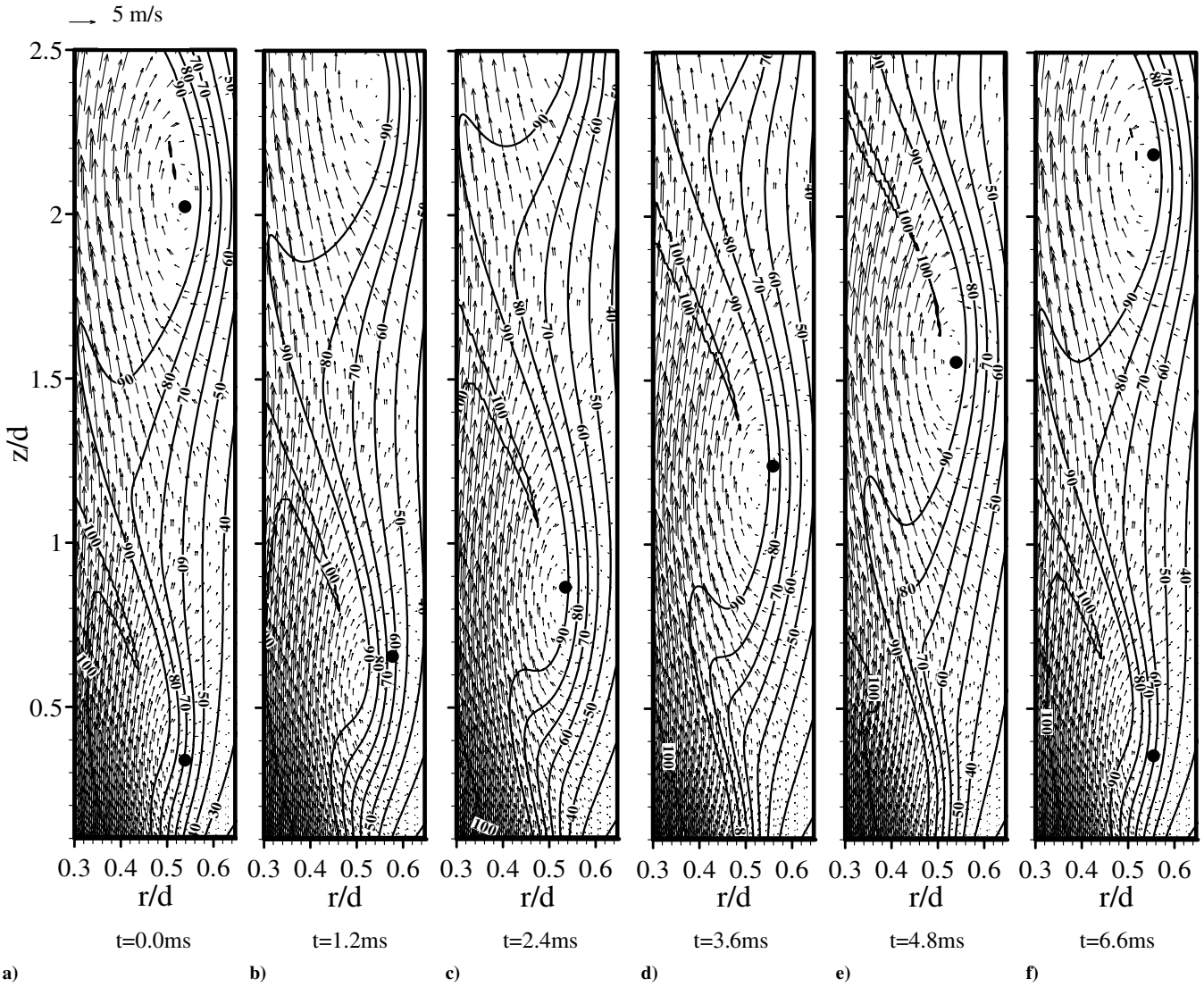

Fig. 6 Velocity vectors superimposed by contours of helium mole percentage during an oscillation cycle in Earth gravity for the inertial jet: $Ri = 0.018$, $Re = 800$, $d = 14.5$ mm (Case 2).

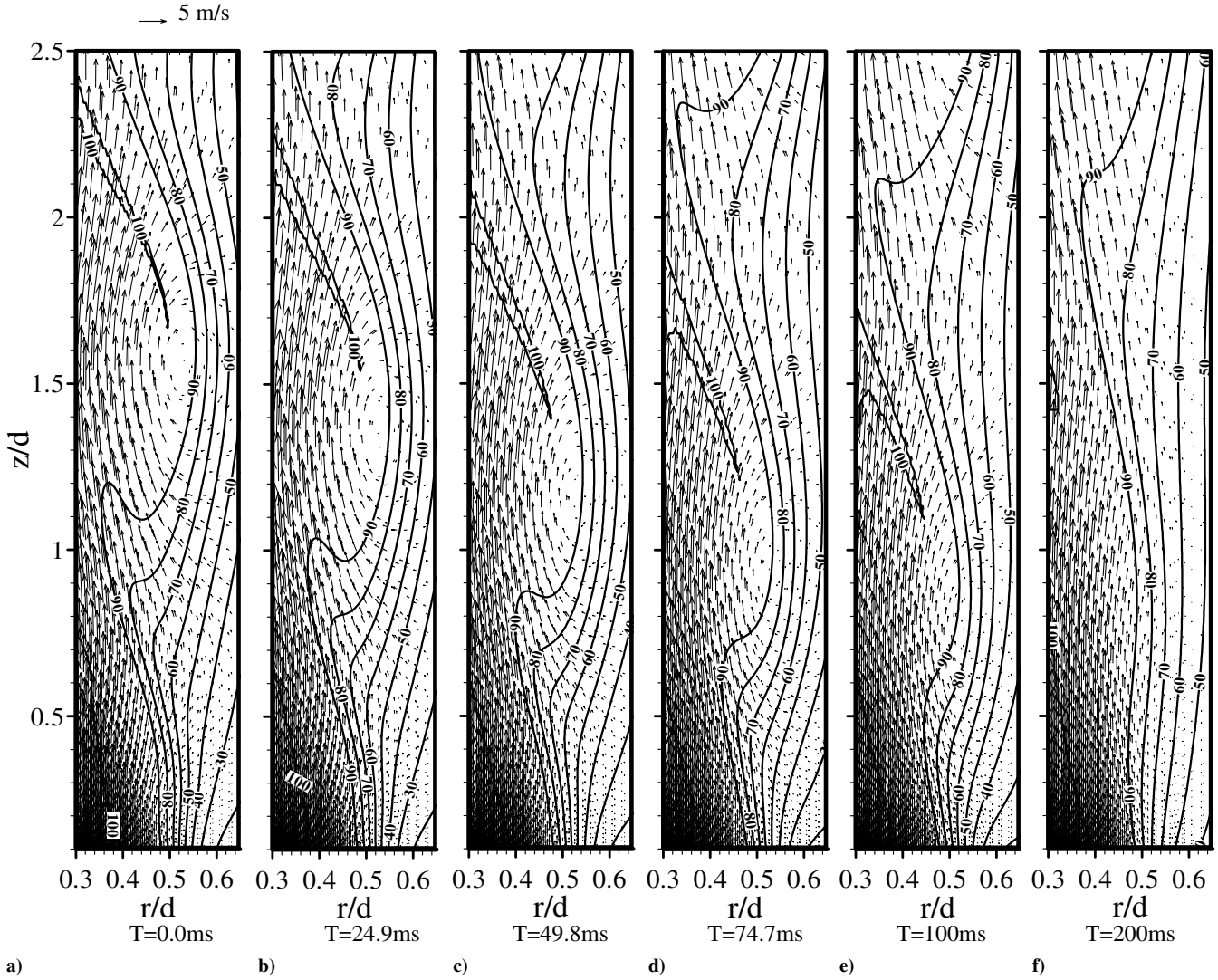

Fig. 7 Velocity vectors superimposed by contours of helium mole percentage during the change from Earth gravity to microgravity for the inertial jet: $Ri = 0.018$, $Re = 800$, $d = 14.5$ mm (Case 2).

3. Temporal Evolution of Axial Velocity and Concentration Fields

Figure 8 shows time trace plots of helium mole percentage and axial velocity at selected locations during the change from Earth gravity to microgravity. At $z/d = 0.5$, the helium concentration at the jet center remained 100% throughout. Concentration fluctuations for the inertial jet are smaller compared with those for the buoyant jet shown in Fig. 5. Axial velocity at the jet center fluctuates between 13 and 14 m/s in Earth gravity and between 12.5 and 13.5 m/s in

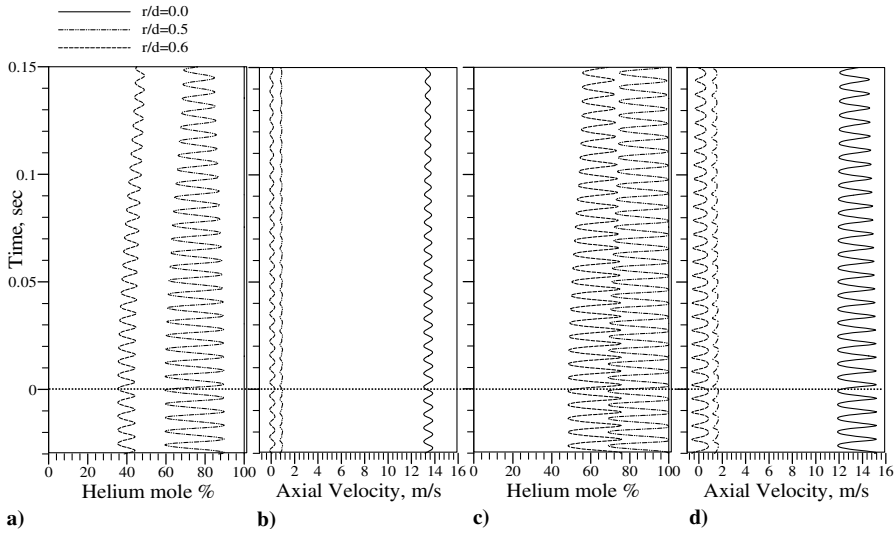

Fig. 8 Time traces of helium mole percentage and axial velocity during the change from Earth gravity to microgravity for the inertial jet: $Ri = 0.018$, $Re = 800$, $d = 14.5$ mm (Case 2) at $z/d = 0.5$ (8a and 8b) and $z/d = 2.0$ (8c and 8d).

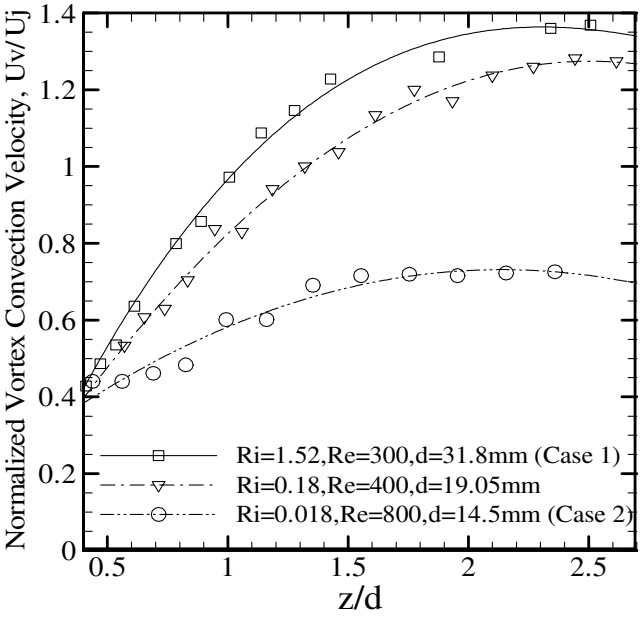

Fig. 9 Vortex convection velocity normalized by the average jet exit velocity U_v/U_j.

microgravity. At the downstream location, $z/d = 2.0$, the axial velocity fluctuates between 12 and 15 m/s in Earth gravity. These fluctuations are slightly smaller in microgravity. The concentration and velocity fields in Fig. 8 reveal that the flow oscillation amplitude decreases in microgravity, ascertaining the importance of buoyancy in inertial low-density gas jets.

C. Comparison of Flow Behavior in Buoyant and Inertial Jets

In this section, buoyant and inertial jet flows are compared to identify similarities and differences in the flow behavior.

1. *Vortex Convection Velocity*

Figure 9 shows the vortex convection velocity U_v normalized by the average jet exit velocity U_j in Earth gravity. The vortex convection velocity was calculated by manually tracking the position of the vortex center at different phases of the oscillation cycle. Results in Fig. 9 show a gradual increase in the vortex convection velocity in the flow direction. The vortex attains a nearly constant velocity in the downstream region. At $z/d = 2.0$, the normalized vortex convection velocity U_v/U_j is 1.35, 1.25, and 0.70, respectively, for $Ri = 1.52$ (Case 1), 0.18, and 0.018 (Case 2). At this axial plane, the vortex convection velocity normalized by the buoyant velocity U_v/U_b was 2.99, 7.83, and 13.84, respectively, for $Ri = 1.52$ (Case 1), 0.18, and 0.018 (Case 2). Here $U_b = \sqrt{gd(\rho_\infty - \rho)/\rho_\infty}$ and $U_j/U_b = 2.22$, 6.42, and 19.2, respectively, for Ri = 1.52 (Case 1), 0.18, and 0.018 (Case 2).

2. *Axial Velocity Profiles*

As stated, buoyancy plays an important role in manifesting the flow instability. Buoyancy is prominent in the jet core for the buoyant jet. However, in the inertial jet, buoyancy effects are confined to the low-momentum region of the jet shear layer. This phenomenon is illustrated by the profiles of instantaneous axial velocity at various radial locations in Fig. 10. The axial velocity was normalized by the jet exit velocity $U_e(r)$ at that particular radial location. The profiles in Fig. 10 show the axial velocity in the streamwise direction at different phases of the oscillation cycles depicted in Figs. 1 and 6.

The normalized axial velocity profiles for the buoyant case (Figs. 10a–10c) show periods of acceleration and deceleration at any given phase. The phases reveal the periodic flow behavior in the near-field region. Along the jet centerline, at phase A, the flow decelerates slightly up to $z/d = 0.8$ and then accelerates rapidly between $z/d =$ 1.0 and 2.0. The velocity peaks at $z/d = 2.0$, which is upstream of the vortex center at $z/d = 2.15$. In phase B, the flow accelerates near the jet exit, where the vortex is formed. In phase C, rapid flow acceleration is observed near the jet exit, with peak normalized axial velocity of 1.25 at $z/d = 0.5$, i.e., upstream of the vortex core at $z/d = 0.80$. Subsequently, the flow decelerates because of the momentum exchange between jet core and vortex. Later in phases D and E, the flow decelerates near the exit but accelerates at

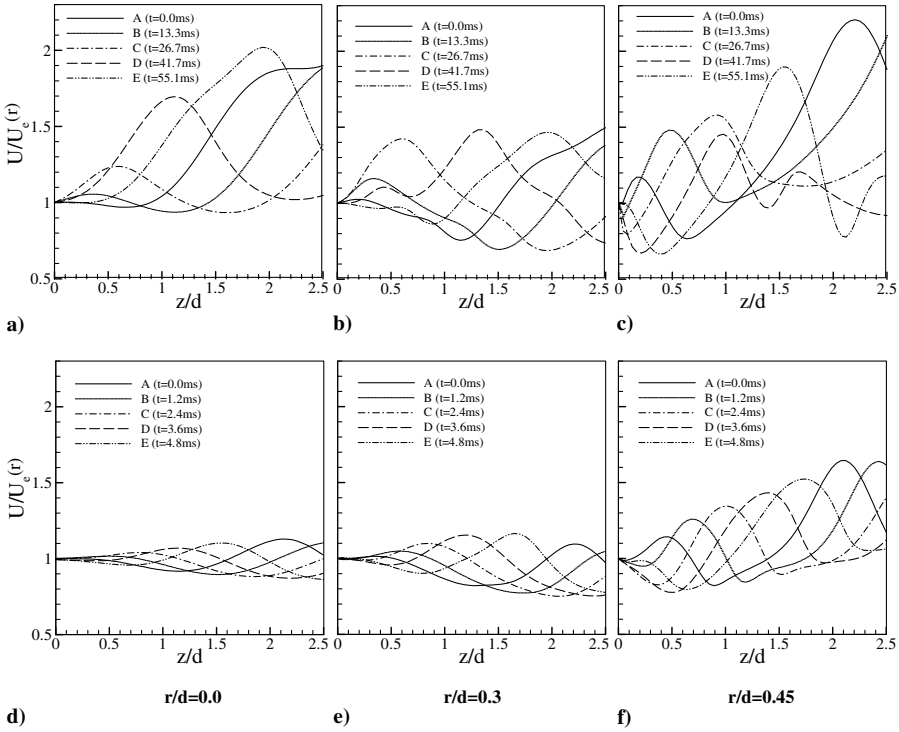

Fig. 10 Axial velocity normalized by the jet exit velocity at the same radial location $[U/U_e(r)]$ for buoyant jet (10a–10c): $Ri = 1.52$, $Re = 300$, $d = 31.8$ mm (Case 1) and inertial jet (10d–10f): $Ri = 0.018$, $Re = 800$, $d = 14.5$ mm (Case 2).

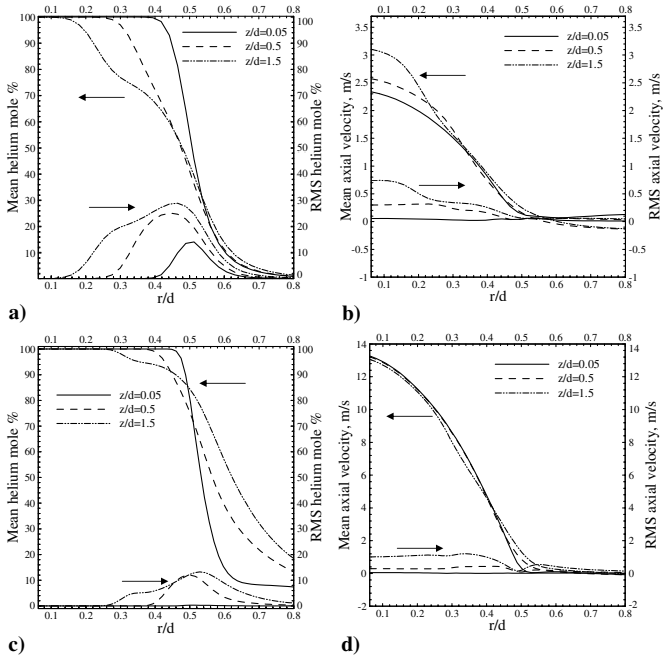

Fig. 11 Profiles of mean and rms helium mole percentage and axial velocity in Earth gravity for buoyant jet (11a and 11b): $Ri = 1.52$, $Re = 300$, $d = 31.8$ mm (Case 1) and inertial jet (11c and 11d): $Ri = 0.018$, $Re = 800$, $d = 14.5$ mm (Case 2).

downstream locations. Note that the normalized peak axial velocity increases to about 1.7 in phase D and to 2.0 in phase E. A common feature is the flow acceleration upstream of the vortex center and deceleration downstream of it. The inertial jet shows a similar behavior. However, the velocity profiles are elongated implying that the velocity peaks farther downstream. The maximum normalized axial velocity is within 1.1 in all phases.

At $r/d = 0.3$, both buoyant and inertial jets exhibit flow acceleration and deceleration near the vortex region. The peak normalized axial velocity decreases from 2.0 at $r/d = 0.0$ to 1.4 at $r/d = 0.3$ for the buoyant jet. However, it increases from 1.1 at $r/d = 0.0$ to 1.2 at $r/d = 0.3$ in the inertial jet. These results illustrate greater importance of buoyancy in the inertial jet at $r/d = 0.3$. At $r/d = 0.45$, both buoyant and inertial jets show large increases in the normalized axial velocity because of the smaller initial momentum in the shear layer region near the jet exit. The flow acceleration signified by the peak axial velocity is similar for buoyant and inertial jets at this radial location ($r/d = 0.45$).

3. *Mean and RMS Flow Structure*

The oscillating flow field of buoyant and inertial jets is compared in Fig. 11 using the mean and rms profiles of helium mole percentage and axial velocity at several axial locations. Near the jet exit at $z/d = 0.05$, the mean concentration shows a top hat profile with finite shear layer thickness. Pure helium is present up to $r/d = 0.38$ for the buoyant jet and up to $r/d = 0.46$ for the inertial case. A steep reduction in helium concentration occurs thereafter. The jet extends to $r/d \cong 0.8$ for the buoyant case and to $r/d > 0.8$ for the inertial case, indicating greater radial expansion at small Richardson numbers (or higher Reynolds number). Thus, the radial diffusion of helium in the near-field is inhibited by strong buoyant acceleration in the buoyant jet.

At $z/d = 0.5$, the mean helium concentration at $r/d = 0.5$ reduces to 50% for the buoyant jet and to 75% for the inertial jet, suggesting greater radial mixing for the former case. Farther downstream at $z/d = 1.5$, helium concentration profiles show an inflection point associated with the vortex at $r/d = 0.29$ for the buoyant jet and at $r/d = 0.33$ for the inertial jet. The concentration gradient near the inflection point is higher for the buoyant jet as compared with the inertial jet.

The rms concentration profiles show large fluctuations near the jet exit for the buoyant jet. The peak rms concentration of 14% at $z/d = 0.05$ increases to 25% at $z/d = 0.5$ and to 29% at $z/d = 1.5$. The location of the peak rms concentration shifts inwards in the flow direction, which is consistent with the contraction of the jet as the vortex propagates downstream. In agreement with experiments [12], the helium concentration fluctuations confined to a wake region ($0.4 < r/d < 0.6$) near the jet exit broaden in the flow direction and contaminate a greater portion of the flow at $z/d > 1.0$. For the inertial jet, the helium concentration fluctuations are negligible at $z/d = 0.05$. The peak rms helium concentration of 10% at $z/d = 0.5$ increases to 12% at $z/d = 1.5$. Smaller fluctuations signify poor scalar mixing in the inertial jet.

Mean axial velocity at $z/d = 0.05$ shows a typical parabolic profile at the tube exit for both buoyant and inertial jets. For the buoyant jet, the axial velocity at the jet centerline increases from 2.4 m/s at $z/d = 0.05$ to 2.6 m/s at $z/d = 0.5$, and to 3.1 m/s at $z/d = 1.5$, indicating strong buoyant acceleration. However, the buoyant acceleration is confined mainly to $r/d < 0.3$. In the inertial jet, the mean axial velocity is nearly the same at all axial locations. The rms axial velocity profiles show negligible fluctuations near the jet exit ($z/d = 0.05$) for both cases. The peak fluctuations increase in the flow direction. For the buoyant jet, the peak rms velocity of 0.3 m/s at $z/d = 0.5$ increases to 0.75 m/s at $z/d = 1.5$. The corresponding values for the inertial jet are 0.3 m/s at $z/d = 0.5$ and 1.0 m/s at $z/d = 1.5$. Note that the rms axial velocity decreases from the centerline towards the boundary plane for the buoyant jet. In contrast, the rms axial velocity is nearly constant up to $r/d \cong 0.4$ for the inertial jet.

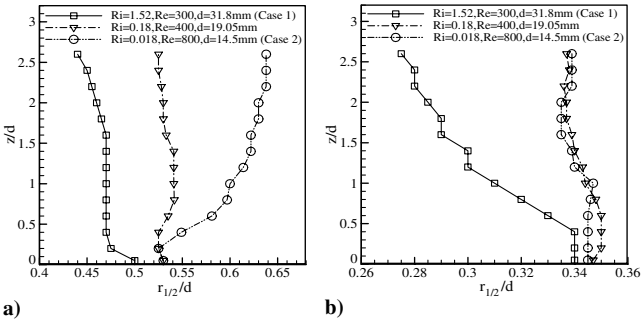

Fig. 12 Jet half radius determined from a) helium concentration and b) axial velocity profiles.

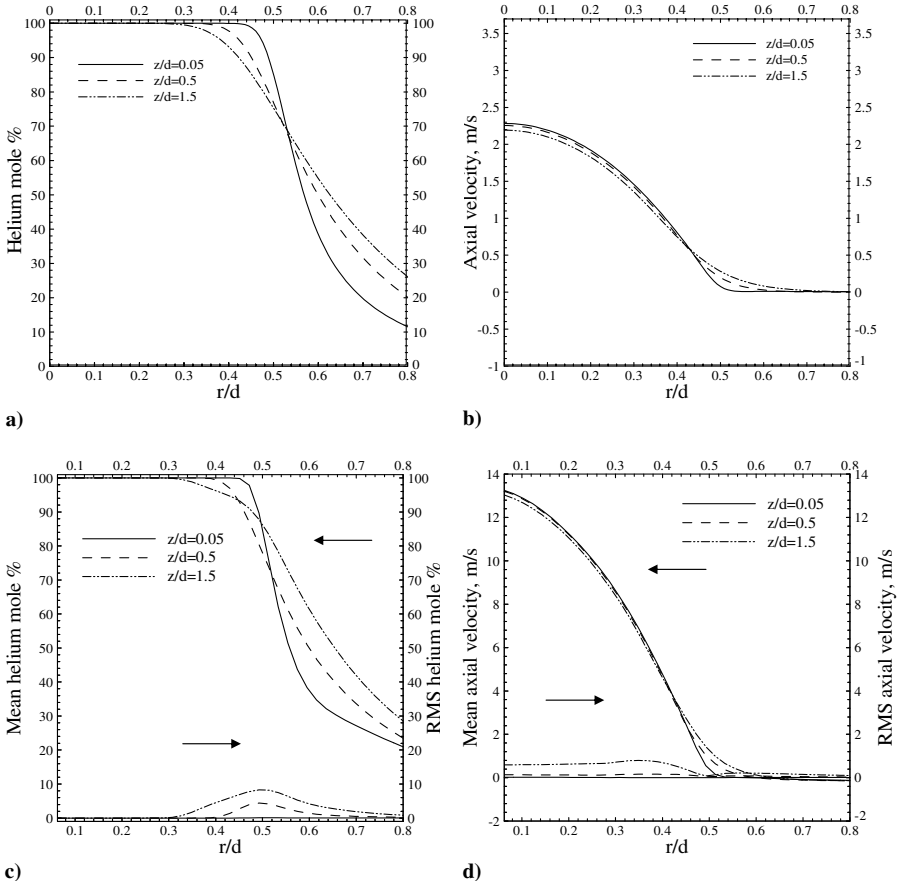

Fig. 13 Profiles of helium mole percentage and axial velocity in microgravity for buoyant jet (13a and 13b): $Ri = 1.52$, $Re = 300$, $d = 31.8$ mm (Case 1) and inertial jet (13c and 13d): $Ri = 0.018$, $Re = 800$, $d = 14.5$ mm (Case 2).

4. Jet Half Radius

As discussed, the jet width increased with increasing initial jet momentum (or the jet Reynolds number). This behavior is quantified by the jet half radius computed at several axial locations; here the jet half radius $r_{1/2}$ is the radial location where the helium mole fraction or the axial velocity is half of that at the jet center. Figure 12 plots the jet half radius normalized by the tube inside diameter, determined from helium concentration and axial velocity profiles. Results in Fig. 12a show that the scalar jet half radius (based on helium concentration profiles) in the axial direction decreases for the buoyant jet, increases for the inertial jet, and remains nearly constant for $Ri = 0.18$, $Re = 400$, and $d = 19.05$ mm. The jet half radius determined from axial velocity profiles, shown in Fig. 12b, also decreases in the axial direction for the buoyant jet, but remains nearly constant for the inertial jet. In a buoyant jet, the ambient fluid is entrained into the jet core because of the rapid acceleration. Consequently, the radial expansion of the jet is constrained and the mixing between jet and ambient fluids is enhanced. In contrast, the high momentum of the inertial jet limits buoyant acceleration, and hence, the penetration of the ambient fluid into the jet core. Thus, the jet half radius is greater because the jet core is less contaminated by the ambient fluid.

5. Flow Behavior in Microgravity

Radial profiles of axial velocity and helium concentration in microgravity are presented in Fig. 13 for buoyant and inertial jets. These profiles were obtained after the jet adapted to the change in gravity. In microgravity, the jet assumed steady, nonoscillatory structure for the buoyant case and an oscillatory flow for the inertial jet. For both cases, the jet width increased with reduction in gravity. For the buoyant jet, the helium concentration at $r/d = 0.7$ is less than 5% in Earth gravity and between 10 and 30% in microgravity. The corresponding values for the inertial jet are between 10 and 20% in Earth gravity and between 20 and 30% in microgravity. Figure 13 shows that the oscillation amplitude for the inertial jet is smaller in microgravity compared with that in Earth gravity. The increase in the radial extent of the jet in microgravity signifies greater role of molecular diffusion in the absence of buoyancy, a well-known phenomenon in flames [25].

IV. Conclusions

A laminar, time-dependent, axisymmetric numerical model was developed and validated to predict the flow structure of low-density gas jets. The CFD-based model was used to simulate buoyant and inertial jets in Earth gravity and microgravity. The major conclusions of the study are summarized as follows:

1) Both buoyant and inertial jets exhibited self-excited periodic oscillations in Earth gravity. The oscillation frequency was higher, the oscillation amplitude was smaller, and oscillations were confined to a narrower region in the inertial jet as compared with the buoyant jet.

2) The buoyant jet depicted flow oscillations for a brief period during the change from Earth gravity to microgravity. The jet eventually attained a steady, columnar structure in microgravity, signifying that the flow oscillations were buoyancy induced.

3) The inertial jet exhibited a reduction in the oscillation amplitude during the change from Earth gravity to microgravity. However, the flow oscillated at the same frequency in both Earth gravity and microgravity.

4) The jet width in Earth gravity increased with increasing initial jet momentum. This unusual behavior of low-density gas jets was explained by the buoyant acceleration of the jet core and its interaction with the toroidal votex.

5) The jet width increased with reduction in gravity, signifying a greater role of molecular diffusion in microgravity.

Acknowledgment

This work was supported by the Physical Sciences Division of NASA's office of Biological and Physical research under grant NNC04GA22G.

References

[1] Fay, J. A., "Buoyant Plumes and Wakes," *Annual Review of Fluid Mechanics*, Vol. 5, 1973, pp. 151–160.

[2] Morton, B. A., "Forced Plumes," *Journal of Fluid Mechanics*, Vol. 5, 1959, pp. 151–159.

[3] List, E. L., "Turbulent Jets and Plumes," *Annual Review of Fluid Mechanics*, Vol. 14, 1982, pp. 189–212.

[4] Papanicolaou, P. A., and List, E. L., "Investigations of Round Vertical Turbulent Buoyant Jets," *Journal of Fluid Mechanics*, Vol. 195, 1988, pp. 342-391.

[5] Dai, Z., Tseng, L. K., and Faeth, G. M., "Structure of Round, Fully Developed, Buoyant Turbulent Plumes," *Journal of Heat Transfer*, Vol. 116, No. 2, 1994, pp. 409–417.

[6] So, R. M. C., Zhu, J. Y., Otugen, M. V., and Hwang, B. C., "Some Measurements in a Binary Gas Jet," *Experiments in Fluids*, Vol. 9, No. 5, 1990, pp. 273–284.

[7] Subbarao, E. R., and Cantwell B. J., "Investigation of a Co-Flowing Buoyant Jet: Experiments on the Effects of Reynolds number and Richardson number," *Journal of Fluid Mechanics*, Vol. 245, 1992, pp. 69–90.

[8] Hamins, A., Yang, J. C., and Kashiwagi, T., "An Experimental Investigation of the Pulsating Frequency of Flames," *Proceedings of the Combustion Institute*, Vol. 24, 1992, pp. 1695–1705.

[9] Cetegen, B. M., and Kasper, K. D., "Experiments on the Oscillatory Behavior of Buoyant Plumes of Helium and Helium–Air Mixtures," *Physics of Fluids*, Vol. 8, No. 11, 1996, pp. 2974–2984.

[10] Cetegen, B. M., "Behavior of Naturally Unstable and Periodically Forced Axisymmetric Buoyant Plumes of Helium and Helium–Air Mixtures," *Physics of Fluids*, Vol. 9, No. 12, 1997, pp. 1–11.

[11] Cetegen, B. M., "Measurements of Instantaneous Velocity Field of a Non-Reacting Pulsating Buoyant Plume by Particle Image Velocimetry," *Combustion Science and Technology*, Vol. 123, Nos. 1–6, 1997, pp. 377–387.

[12] Pasumarthi, K. S., and Agrawal, A. K., "Schlieren Measurements and Analysis of Concentration Field in Self-Excited Helium Jets," *Physics of Fluids*, Vol. 15, No. 12, 2003, pp. 3683–3692.

[13] Yep, T. W., Agrawal, A. K., and Griffin, D. W., "Gravitational Effects on Near-Field Flow Structure of Low Density Gas Jets," *AIAA Journal*, Vol. 41, No. 10, 2003, pp. 1973–1979.

[14] Sreenivasan, K. R., Raghu, S., and Kyle, D. M., "Absolute Instability in Variable Density Round Jets," *Experiments in Fluids*, Vol. 7, No. 5, 1989, pp. 309–317.

[15] Monkewitz, P. A., Bechert, D. W., Bariskov, B., and Lehmann, B., "Self Excited Oscillations and Mixing in a Heated Round Jet," *Journal of Fluid Mechanics*, Vol. 213, 1990, pp. 611–639.

[16] Kyle, D. M., and Sreenivasan, K. R., "The Stability and Breakdown of a Round Variable Density Jet," *Journal of Fluid Mechanics*, Vol. 249, 1993, pp. 619–664.

[17] Richards, C. D., Breuel, B. D.,Clark, R. P., and Troutt, T. R., "Concentration Measurements in a Self-Excited Jet," *Experiments in Fluids*, Vol. 21, No. 2, 1996, pp. 103–109.

[18] Yildirim, B. S., and Agrawal, A. K., "Full-Field Measurements of Self-Excited Oscillations in Momentum-Dominated Helium Jets," *Experiments in Fluids*, Vol. 38, No. 2, 2005, pp. 161–173.

[19] Pasumarthi, K. S., "Buoyancy Effects on Flow Structure and Instability of Low-Density Gas Jets," Doctoral Dissertation, Univ. of Oklahoma, Norman, OK, 2004.

[20] Pasumarthi, K. S., and Agrawal, A. K., "Buoyancy Effects on Flow Transition in Low-Density Inertial Gas Jets," *Experiments in Fluids*, Vol. 38, No. 4, 2005, pp. 541–544.

[21] Mell, W. E., McGrattan, W. B., and Baum, H. R., "Numerical Simulation of Combustion in Fire Plumes," *Proceedings of the Combustion Institute*, Vol. 26, 1996, pp. 1523–1530.

[22] Soteriou, M. C., Dong, Y., and Cetegen, B. M., "Lagrangian Simulation of the Unsteady Near-field Dynamics of Planar Buoyant Plumes," *Physics of Fluids*, Vol. 14, No. 9, 2002, pp. 3118–3140.

[23] Satti, R. P., and Agrawal, A. K., "Flow Structure in the Near-Field of Buoyant Low-Density Gas Jets," *International Journal of Heat and Fluid Flow*, Vol. 27, No. 2, 2006, pp. 336–347.

[24] Katta, V. R., and Goss, L. P., "Numerical Investigations of Transitional H_2/N_2 Jet Diffusion Flames," *AIAA Journal*, Vol. 32, No. 1, 1994, pp. 84–94.

[25] Sato, H., Kushida, G., Amagai, K., and Arai, M., "Numerical Analysis of the Gravitational Effect on the Buoyancy-Driven Fluctuations in Diffusion Flames," *Proceedings of the Combustion Institute*, Vol. 29, 2002, pp. 1671–1678.

[26] Kyle, D. M., "The Instability and Breakdown of a Round Variable-Density Jet," Doctoral Dissertation, Yale Univ., New Haven, CT, 1991.

[27] Bird, R. B., Stewart, W. E., and Lightfoot, E. N., *Transport Phenomena*, 1st ed., Wiley, New York, 1960.

[28] Gaenkoplis, C. J., "Mass Transport Phenomena," Holt, Rinehart, and Winston, New York, 1972.

[29] Fluent 6.0, User's Guide, Fluent Inc. Lebanon, NH 1-4, 2003.

[30] Shenoy, A. K., Agrawal, A. K., and Gollahalli, S. R., "Quantitative Evaluation of Flow Computations by Rainbow Schlieren Deflectometry," *AIAA Journal*, Vol. 36, No. 11, 1998, pp. 1953–1960.

S. Aggarwal
Associate Editor